RESISTANCE SPOT WELDING OF GALVANIZED ADVANCED HIGH STRENGTH DP800 STEEL

GELİŞMİŞ YÜKSEK DAYANIMLI DP800 ÇELİĞİNİN ELEKTRİK DİRENÇ PUNTA KAYNAĞI

BURAK ARSLAN

ASSIST. PROF. DR. MEHMET OKAN GÖRTAN

Supervisor

Submitted to

Graduate School of Science and Engineering of Hacettepe University

as a Partial Fulfillment to the Requirements

for the Award of the Degree of Master of Science

in Mechanical Engineering

2024

ABSTRACT

RESISTANCE SPOT WELDING OF GALVANIZED ADVANCED HIGH STRENGTH DP800 STEEL

Burak ARSLAN

Master of Science, Department of Mechanical Engineering

Supervisor: Prof. Dr. Mehmet Okan GÖRTAN

May 2024, 35 Pages

The aim of the study is to investigate the effect of welding current on weld quality of DP800 joints obtained using resistance spot welding method. Electrogalvanized 1 mm thick DP800 steel sheets were used as the workpiece. Resistance spot welding method was applied using welding current varying between 6.5 kA and 12.0 kA with a step size of 0.5 kA. Electrode force and weld time kept constant at 3.1 kN and 14 cycle, respectively. Welded samples were subjected to several tests in order to analyze the weld quality and mechanical performance of the joints in each welding current level. Microstructure, microhardness and nugget geometry on the weld cross sectioning was examined. Afterwards, weld joints were exposed to tensile-shear test. Mechanical properties and failure modes of the fractured joints in tensile loading were analyzed. As a result, it was observed the welding current has a great impact on weld quality. Increase in welding current up to expulsion limit (9.0 kA) resulted in an increase in nugget size and an improvement in the mechanical properties of the joints. However, welding current usage beyond the expulsion limit resulted in inconsistent nugget formation and therefore deviation in the mechanical properties of the joints. As a result, it was found the optimum

nugget geometry and the mechanical properties in the DP800 joints are obtained using 9.0 kA welding current.

Keywords: Resistance Spot Welding, Advanced High Strength Steel, DP800, Microstructure, Tensile-Shear Strength, Failure Energy, Failure Mode Analysis

ÖZET

GELİŞMİŞ YÜKSEK DAYANIMLI DP800 ÇELİĞİNİN ELEKTRİK DİRENÇ PUNTA KAYNAĞI

Burak ARSLAN

Yüksek Lisans, Makina Mühendisliği Bölümü

Tez Danışmanı: Prof. Dr. Mehmet Okan GÖRTAN

Mayıs 2024, 35 Sayfa

Çalışmanın amacı, elektrik direnç punta kaynağı yöntemi kullanılarak elde edilen DP800 kaynak bağlantılarının kalitesine kaynak akımının etkisinin araştırılmasıdır. İş parçası olarak electrogalvanizli 1 mm kalınlığında DP800 çelik saclar kullanılmıştır. Elektrik direnç punta kaynağı yöntemi 6.5 kA ile 12.0 kA arasında 0.5 kA adım büyüklüğünde değişen kaynak akımı kullanılarak uygulanmıştır. Elektrot kuvveti ve kaynak süresi sırasıyla 3.1 kN ve 14 çevrimde sabit tutulmuştur. Kaynaklanan numuneler kaynak kalitesini ve bağlantıların mekanik performansını her kaynak akımı seviyesinde analiz etmek için çeşitli testlere tabi tutulmuştur. Kaynak kesitinde mikroyapı, mikro sertlik ve çekirdek geometrisi incelenmiştir. Daha sonra, kaynak bağlantıları çekme-makaslama testine tabi tutulmuştur. Çekme yüklemesinde kırılan bağlantıların mekanik özellikleri ve kırılma tipleri analiz edilmiştir. Sonuç olarak kaynak akımının kaynak kalitesine büyük etkisi olduğu görülmüştür. Kaynak akımının taşma sınırına (9.0 kA) kadar olan artışı çekirdek boyutunun artmasına ve bağlantıların mekanik özelliklerinin iyileşmesine sebep olmuştur. Ancak, taşma sınırının ötesinde kaynak akımı kullanımı tutarsız çekirdek oluşumuna ve dolayısıyla bağlantıların mekanik özelliklerinde sapmaya neden olmuştur.

Sonuç olarak DP800 bağlantılarında optimum çekirdek geometrisinin ve mekanik özelliklerin 9.0 kA kaynak akımı kullanılarak elde edildiği bulunmuştur.

Anahtar Kelimeler: Elektrik Direnç Punta Kaynağı, Gelişmiş Yüksek Dayanımlı Çelik, DP800, Mikroyapı, Çekme Dayanımı, Kırılma Enerjisi, Kırılma Tipi Analizi

ACKNOWLEDGEMENTS

First of all, I would like to thank my supervisor Assist. Prof. Dr. Mehmet Okan GÖRTAN for his guidance in this academic study. Thanks to his deep knowledge, I was able to find qualified answers to all my questions.

I would like to thank my colleagues, Ford Otosan engineers, for their valuable support during this thesis study.

I would like to thank my dear friends Berkay BARIN, Onur TANRISEVER, Volkan ERTOĞAN, Malik TOPLU, Zafer Cem ÖZCAN and Eren Cem GÖKSÜLÜK for their continuous support during this stressful research period. Thanks to them, I was highly motivated for this academic research.

Above all, I would like to express my sincere gratitude to my family Mehmet ARSLAN, Vahide ARSLAN, Damla ARSLAN and Murat ARSLAN for their unwavering support in this though thesis work. They always stand with me in all the challenges I face.

TABLE OF CONTENT

LIST OF FIGURES

LIST OF TABLES

SYMBOLS AND ABBREVIATIONS

Symbols

Q: Heat

I: Welding Current

R: Resistance

t: Time

Abbreviations

RWS: Resistance Spot Welding

AHSS: Advanced High Strength Steels

DP: Dual Phase

FZ: Fusion Zone

HAZ: Heat Affected Zone

TRIP: Transformation Induced Plasticity

Q&P: Quenching and Partitioning

LME: Liquid Metal Embrittlement

AWS: American Welding Society

SEM: Scanning Electron Microscope

ICHAZ: Inter-critical Heat Affected Zone

UCHAZ: Upper-critical Heat Affected Zone

1. INTRODUCTION

Production methods are constantly being improved in many sectors. Especially in automotive engineering, production methods forced to be time-efficient in order to obtain high production rates. Resistance spot welding (RSW) is one of the welding methods that provides high production rate, particularly used in the automotive industry. RSW is a lap joint welding method that uses electric current to generate heat input needed to weld the metal sheets. The heat input is obtained with the electric current flow against the material resistance.

There are many advantages of the RSW such as high production rate and low operation cost. RSW is a reliable manufacturing method since the process can be automated. Dissimilar materials can also be used in the spot welding process. Because of these advantages, RSW is the dominant joining method in the automotive industry. Modern vehicles consist of thousands of spot welds [1]. However, there are also limitations of the process. Initial cost of the spot welding equipment is high. Besides, RSW is not a proper welding method to use with thicker sheets [2].

In addition to the basic features of the RSW, its ability to work with new generation steels is one of the features that makes the process more preferable. Advanced high strength steels (AHSS) are the new generation steels currently used in spot welding of modern vehicles. AHSS usage in automotive engineering provides high strength level, as well as good formability, which results with improved crash safety even with the reduced vehicle weights. In addition to the safety, the use of AHSS in modern vehicles reduces fuel consumption and environmental impact of the process, thanks to weight lowering [3, 4].

RSW of galvanized DP800 dual phase (DP) steel has been studied in thesis work. Motivation of the study is to examine the weldability of the advanced galvanized DP800 steel and to determine the key factors affecting the mechanical properties of the spot welds. Effects of welding parameters on failure modes and weld quality will be discussed in following chapters. Outline of the thesis will be followed by the literature review, explanation of experimental studies, discussion of the results and the conclusion section.

2. LITERATURE REVIEW

2.1 Resistance Spot Welding Process

RSW is a metallurgical process in which thin metal sheets are welded [5]. In RSW process, required heat input to melt the metal sheets is generated as a result of electric current flow through the sheets. Schematic process diagram of RSW is shown in Figure 2.1.1.

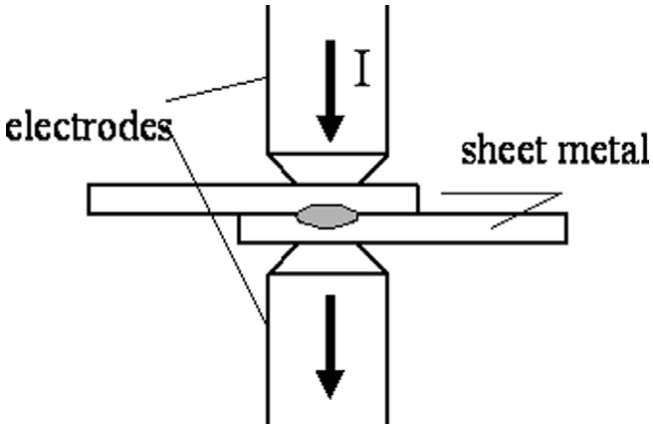

Figure 2.1.1 Resistance spot welding process illustration [6]

First of all, metal sheets should be placed appropriately on the welding fixture that is touching the lower electrode. Two copper-based electrodes used in RSW to clamp the metal sheets and transmit the electric current. In the beginning of spot welding cycle, upper electrode moves down to contact the metal sheet while the lower electrode is stationary. Then, electric current starts to flow through the workpiece. Required heat input to melt the metal is generated by the encounter of electric current and material resistance.

In addition to the welding current, welding time is a welding parameter that has a great impact on the heat input and therefore on the mechanical properties of the spot welds. Joule's Law is utilized to explain the heat generation in RSW [7]

$$Q = I^2 * R * t \quad (1)$$

In the equation 1, Q, I, R and t represent the total heat input (Joule), welding current (Ampere) total resistance of the metal sheet stack (Ohm) and welding time (second) respectively. Total heat input is proportional to the welding time, resistance and the square of the welding current. Total heat, in joule, in the above equation represents the total

amount of heat given into the system via power supply. It does not correspond to the energy received by the molten metal at faying interface of metal sheets. Since the electric current flows through the path between the electrodes, there will be heat generation through the full path consisting multiple resistance properties.

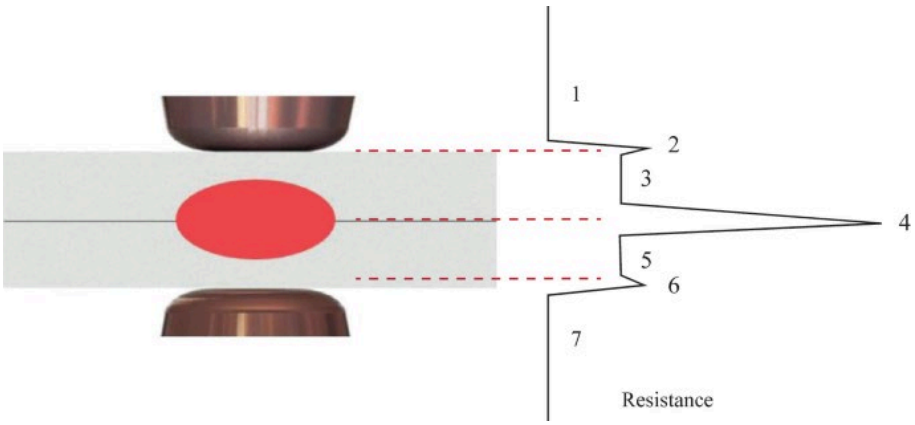

Figure 2.1.2 Resistance plot across the resistance spot welding path [7]

Figure 2.1.2 shows the resistance spot welding illustration and the resistance plot covering all resistance properties between the upper and lower electrodes. 1 and 7 in Figure 2.1.2 represent the bulk resistance of copper electrodes while 3 and 5 represent the bulk resistance of metal sheets. Apart from the bulk resistances there are also contact resistances at the copper-sheet interfaces (2, 6) and sheet-sheet interface (4) [7]. Molten metal is symbolized with the red elliptical in Figure 2.1.2. Since the resistance is highest at the sheet-sheet interface, highest heat generation is observed in this elliptical region which is called as fusion zone (FZ). Therefore, in a successful spot welding process metal in the FZ melts and solidifies to form a nugget. Total heat input (Q) corresponds to the heat obtained through the all resistance path (resistor 1 to 7). Therefore, there is a heat loss which is the difference between the heat input and the heat used to melt the metal in FZ to form a nugget [8]. Figure 2.1.2 represents the heat generation mechanism prior to nugget formation [7].

Weld quality of the spot welds is not only affected by the heat generated in the FZ. Mechanical properties of the spot welds are also determined by the electrode force. During the welding cycle, electrode force is applied on metal sheets to create clamping and proper contact on sheets so that the electric current flow is secured. As the electrode

force increases, surface roughness of the workpiece is suppressed resulting in decreased contact resistance. As we learned from Joule's Law, heat generation will be lowered on the contact surface of metal sheets with decreased contact resistance while the rest of the welding parameters remain same. Reducing the contact resistance up to a certain level is essential for a consistent welding process despite the heat loss in FZ [7, 9].

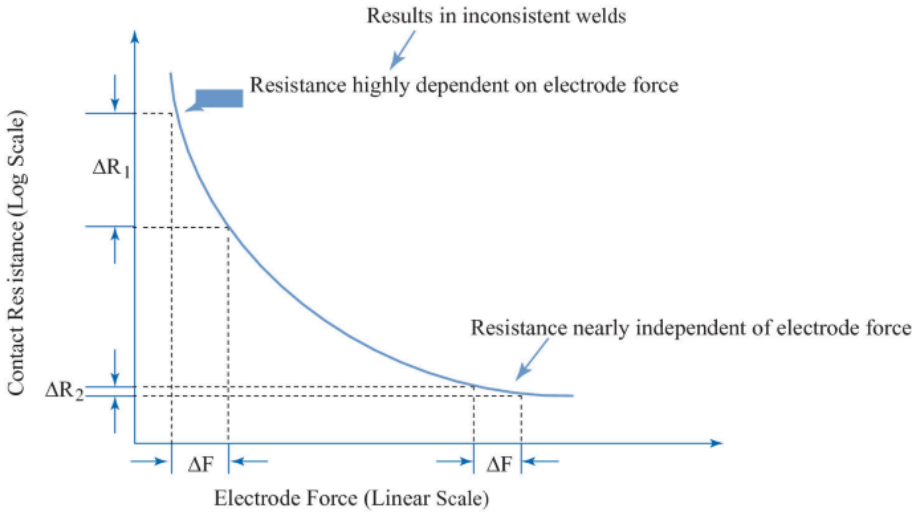

Figure 2.1.3 Electrode force effect on contact resistance [7]

Figure 2.1.3 shows there is huge dependency on electrode force in spot welding at very low electrode forces since small change in force results with huge difference in contact resistance. In order to decrease the variation in heat generation, dependency on electrode force should be decreased. Besides, electrode force suppresses the liquid metal pressure of molten metal in FZ [9]. Liquid metal escape from the contact of sheet surfaces, which is called expulsion, is an expected result with insufficient electrode force implementation. However, further increase in electrode force results with excessive indentation on electrode metal contact surface. Therefore, optimization of welding parameters is the key to obtain better weld quality.

2.2 Spot Weld Attributes

Macrostructure of the spot welds consist of multiple zones such as base metal, heat affected zone (HAZ), and fusion zone (FZ). Workpiece is under heat treatment in RSW. Microstructure of the workpiece material, so that the macrostructure also, is changed as

a result of heating and cooling in a short period. Fusion occurs between two metal sheets in the FZ by melting metal as a result of electric current flow against the material resistance. Then, solidification of liquid metal in FZ occurs with a high cooling rate to form a nugget. HAZ is located next to the FZ, which is partially molten region where the grain growth occurs. Temperature in HAZ is between the solidus and liquidus temperatures of the metal. It is a kind of a transition between the FZ and base metal [10]. Figure 2.2.1 illustrates the metallographic sectioning of spot weld.

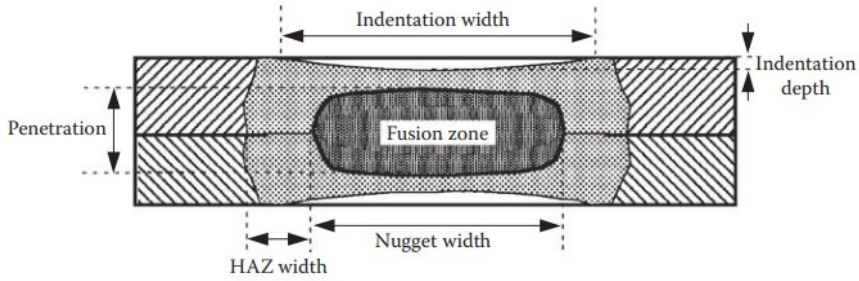

Figure 2.2.1 Cross sectioning of spot weld macrostructure [11]

Weld quality is highly dependent on geometrical attributes and the strength of the spot weld. Nugget width is the most common reviewed geometrical feature of the spot welds to evaluate the weld quality. Larger fusion zone can be obtained with an increased nugget width. However, nugget width is not the only geometrical attribute determining the size of the area of adhesion. Penetration size also determines the size of the fusion area. Higher load bearing capability can be achieved with a larger weld for the same workpiece materials if the defect rate variation in the nuggets is ignored. Besides the geometrical features of the spot welds, strength is a welding characteristic determining the weld quality. Tensile-shear test is the most common method used to measure the tensile-shear strength of the spot welds [11].

In addition, expulsion, which is the material escape from FZ, is mostly observed and undesired phenomenon in RSW. Expulsion occurs due to disruption of the mechanical equilibrium between the liquid pressure of the molten metal in the FZ and electrode pressure mostly because of the excessive heat input or insufficient electrode force. Since the expulsion mostly results in decrease in nugget width and inconsistent mechanical

properties in mass production, it adversely affects the weld quality and limits the weldability of a RSW workpiece.

2.3 Industry Usage of Resistance Spot Welding

RSW is a widely preferred welding method particularly in automotive industry. High production rates can be achieved with RSW since it can have automated. Automatization of the process with robotic control makes the process consistent therefore the reliability is among the advantages of the RSW. Another advantage of the process is low labor cost since the process can be operated by semiskilled operators. RSW method does not require filler material to weld the overlapping sheets. Dissimilar materials can be joined in RSW. However, the process is feasible for only sheet products up to 3 mm thick. One of the other limitations of the process other than the material thickness is geometrical constraints of the tools and products. Accessibility of the sheets from both sides is a requirement to be able to hold and weld the metal sheets in RSW [12]. The geometric limitations of the tools must be taken into account especially when welding the edges of a body.

The RSW method serves in many industries such as medical, defense, electronics, aerospace and automotive. Battery manufacturing, kitchen tool production, wire mesh welding in outdoor fences, automotive body welding is some of the applications of RSW [13-15]. Since the process is efficient in terms of cost and energy, it is frequently used in assemblies where the spot joints are satisfactory.

2.4 Advanced High Strength Steels

Recently, AHSS are the preferable steel type particularly in automotive industry because of their enhanced mechanical properties. Ultra-high strength steels or advanced high strength steels are basically the steels with advanced strength compared to conventional steels. Major difference between the advanced and conventional steels is the microstructure composition. Conventional steels are basically the single-phase steels with relatively low strength. AHSS are the multi-phase steels with an engineered microstructure containing martensite, bainite, austenite additional to the ferrite [16]. Targeted mechanical properties can be achieved with the manipulation of phase proportion and distribution in the alloy composition. Thus, formable steels can be

obtained even with the ultimate strength level. Figure 2.4.1 shows the formability of the conventional and advanced steels.

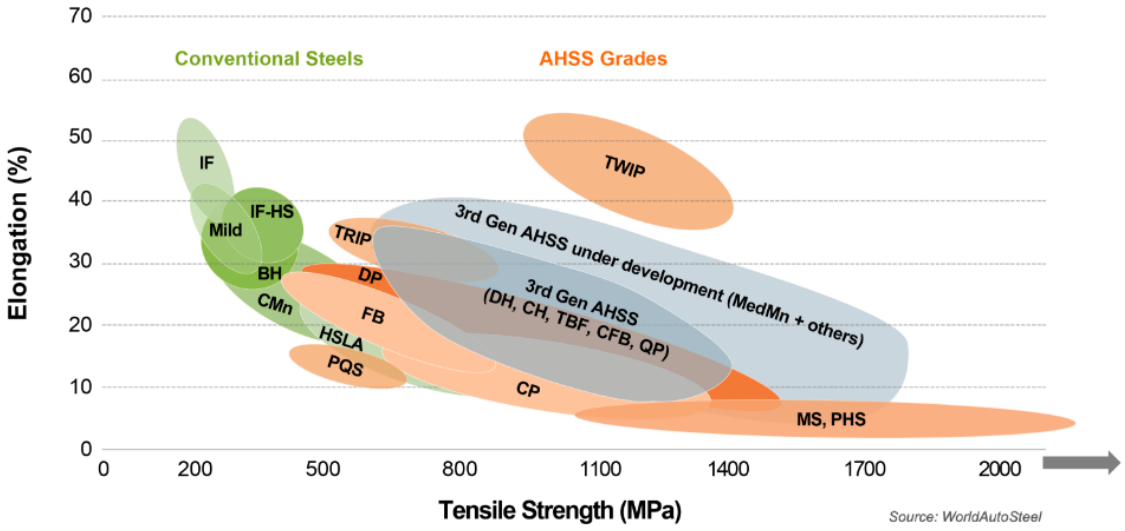

Figure 2.4.1 Global formability diagram of steels [16]

Graph in Figure 2.4.1 shows the elongation rate of the steel grades by tensile strength. DP, TRIP (Transformation Induced Plasticity) steels are some of the first generation AHSS which are commonly reviewed in RSW in terms of weldability. Lately, new third generation AHSS are under development which has high strength as well as enhanced formability [16]. Since elongation is a measure of ductility, it is usually expected to observe decrease in elongation rate of the steel with the increase in strength level. New generation advanced steels are beyond this expectation. Sacrifice of ductility for strength increase is minimized with the third generation advanced steels.

AHSS have higher resistivity than the conventional steels. Therefore, compared to the conventional steels, heat generation requirements of spot welds of AHSS might be satisfied even with decreased welding currents. However, the situation is different when the concern is the electrode force. Since the electrode force is dependent on material strength, higher electrode force is required on AHSS sheets for the same thickness of conventional steel sheets [17]. Welding standards can be used to determine the process parameters. Various welding standards have been reviewed in Kimchi and Philips' book [7].

2.5 Resistance Spot Welding Applications of Advanced High Strength Steels

In 2017, H. L. Jaber et al. investigated the key parameters affecting the mechanical response of spot welds of DP600 steel. In this paper, FZ size, mechanical performance and failure mode of the spot welds has been examined which are three general indexes determining the weld quality. DP600 DP steel sheets with both of 1.5 mm thickness was used as base metal. Experimental method of the study is to increase the welding current from 6.0 kA up to 13.0 kA with a 0.5 kA step size when the cycle time and electrode force remain constant. Therefore, it has been analyzed if there is a significant effect of welding current on resistance spot weld quality of DP600 spot welds. The study proved that FZ size and mechanical performance of the spot welds are highly dependent on welding current. Increasing welding current up to expulsion limit (11.0 kA for the study of Jaber et al.) increased the FZ size, load carrying capacity and energy absorption capability of the spot welds. Further increase in welding current resulted with FZ decrease because of the expulsion. In the research, FZ size was the key factor affecting the quality and mechanical performance of the spot welds since there is a linear relationship with the FZ size and the mechanical response characteristics of the spot welds. In addition, failure mode, the other index affects the mechanical properties of the spot welds, also changed with FZ size. There is a critical FZ size where the transition was observed from interfacial failure to pullout failure. The critical FZ size of the study is 8 mm above which the pullout failure, the preferred failure manner, was obtained [1].

DP600 DP steel sheets with both of 1.6 mm thickness were used in 2019, in the research of Sivaraj et al. The effect of welding current on nugget formation was examined. It was found that the welding current significantly affects the nugget formation and spot weld quality. Welding current was gradually increased with a 5.0 kA interval from 40.0 kA up to 60.0 kA while the electrode force and welding time kept constant. 50.0 kA is the optimum welding current of the study which the proper nugget formation without defects was achieved. Nugget formation cannot be obtained with the 40.0 kA due to low heat input and the FZ size was decreased with the maximum current value of the experiment, 60.0 kA. Meanwhile, maximum tensile shear fracture load (18 kN) and the FZ hardness value (480 HV) were obtained with the 50.0 kA welding current which the largest fusion bond area and the penetration were achieved. Both of interfacial failure and pullout failure modes were observed in the study. Due to HAZ softening, failure occurrence on heat affected zone was also observed [18].

In the research of Jie et al., in 2011, electrode force effect on expulsion with the initially gapped galvanized DP steel DP590 was studied. The gap in advanced steel sheets faying interface is a common issue due to roughness and positioning errors. The study shows the expulsion could be triggered with the increase of the gap between the steel sheets. Therefore, it was searched in the study if the electrode force increment could provide proper contact and eliminate the expulsion risk caused by the gap between the steel sheets. DP590 steel sheets with various thicknesses was used in the study, 0.8, 1.4 and 1.8 mm, and the initial gap spacing was changed from 0 to 2.0 mm. First, the required electrode force to inhibit the expulsion was searched without initial gapping for various sheet thicknesses. These electrode force values for the corresponding sheet thicknesses were not sufficient to prevent the expulsion when the initial gap was applied. Thus, required electrode force to inhibit the expulsion in RSW with initial gap spacing was higher for the same sheet thicknesses. Furthermore, to eliminate the expulsion, more electrode force increment was needed for the thicker sheets even with the same gap spacing. Hence, it was found that the electrode force needed to prevent the expulsion is dependent on both of sheet thicknesses and gap spacing and should be increased with the increase of those [19].

Effect of welding current waveform on expulsion was searched in 2011 by Hwang et al. It was studied if the welding current waveform decrease the expulsion tendency at high welding currents. Al-Si coated steel sheets with a thickness of 1.2 mm and a strength of 1500 MPa were used in the study. Invertor direct current (DC) was used to weld the steel sheets. At the beginning of the study, conventional DC current waveform which includes only heating part during welding time was used to evaluate the weldability of the steel sheets. It has been observed the acceptable welding current range with the conventional welding form is narrow, around 2.0 kA. Maximum welding current limit (6.0 kA), which is the expulsion limit, did not increased even the electrode force was increased. However, maximum acceptable current limit was increased to 7.0 kA from 6.0 kA with the pulse welding current waveform consisting of heating and cooling parts. The study showed that the overheating caused by the welding form increased the expulsion prone especially at high welding currents. Therefore, pulse welding current form can reduce the expulsion risk thanks to cooling part. As a result, acceptable current range was increased with the pulse welding form [20].

In 2020, RSW of new generation quenching and partitioning (Q&P) steel Q&P1180 was studied by Chen et al. Dome-radius electrode and slightly concave electrode, which is achieved by machining of dome-radius electrode with a recess of 0.05 mm depth and 4 mm diameter, were used in the research. Effects of both types of electrode tips on microstructure and tensile-shear properties were compared. Optimal welding currents, 7.5 kA for dome-radius electrode and 10.0 kA for concave electrode, were used in comparison. Similar microhardness distribution and FZ microstructure, mainly in lath martensite form, were obtained in spot welds made with dome-radius and concave electrode. However, different tensile-shear properties were obtained with the two types of electrodes because of thermal & electric field and nugget growth difference. Ability of suppressing the expulsion is higher with the use of concave electrode compared to dome-radius electrode because of the lower current density at early stage and enhanced corona bond strength. Therefore, maximum nugget diameter and tensile-shear peak load were increased with the concave tip design implementation. Welding current range and maximum current limit at which the pullout failure can be achieved without expulsion was also increased with the use of concave electrode. Thanks to the higher maximum current limit and fusion zone size, spot weld made with the conventional dome-radius electrode failed in single-sided pullout failure, while the concave electrode used spot weld failed in double-sided pullout failure mode. As a result, total failure energy increased with the concave electrode tip usage [21].

Liang et al. studied the RSW of dissimilar AHSS in 2015. Microstructure and mechanical performance of spot weld joints consist of dissimilar DP steels were investigated. DP780 and DP600 steels were used as base metals with a thickness of 1.2 mm and 1.5 mm respectively. In microhardness measurement, highest hardness values (~350 HV) were achieved in FZ due to lath-martensite structure occurred as a result of high peak temperature and cooling rate. There was a drop in microhardness values of both steels in HAZ close to the BM. The reason of that is HAZ softening occurred as a result of tempered martensite. Failure modes observed in the research were interfacial failure, partial interfacial failure and pullout failure. In the research, minimum nugget diameter above which the pullout failure was achieved are in consistent with the proposed model of the Pouranvari and Marashi [22]. Expulsion was observed in both of electrode/sheet and faying interface. Expulsion occurrence in faying surface did not prevent the increase of peak load up to approximately 19 kN. Despite of expulsion, thanks to the rise in the

nugget diameter, shear-tensile strength also increased up to a welding current of 11.5 kA. However, further increase in welding current resulted in severe expulsion, mass loss in faying surface and stop of nugget diameter increase. In the study, no findings regarding the influence of expulsion on failure energy were presented by the researchers. Besides, expulsion from faying surface was occurred in all specimens using welding current above 8.0 kA. However, when welding current kept constant at 8.0 kA, expulsion was only observed in very few specimens with the change of electrode force and welding time. Therefore, in the RSW of DP780/ DP600, expulsion was mostly affected by the welding current [23].

In the research of Sun et al., two types of AHSS spot welds were compared in terms of mechanical performance, weld quality. Galvanized 1.6mm thick DP800 sheets and 1.5 mm thick TRIP800 sheets were used separately to obtain spot weld joints consist of similar materials. Targeted FZ size populations were small, nominal and large FZ size populations with 4.9 mm, 6.5 mm and 7.5 mm nugget diameters respectively. Predetermined welding parameters such as electrode force, welding current and welding time were used, that vary for each population, to obtain different size of FZ. Then, effect of FZ size on failure mode, peak load and failure energy of spot welds was examined for each population. It was observed that the failure mode is most effecting factor on peak load and failure energy of DP800 spot welds. Nominal FZ population failed in interfacial failure mode had less failure energy than that small FZ population failed in pullout failure mode, despite increasing FZ size. However, when the spot welds failed in only pullout failure mode were compared, increasing FZ size resulted in increase in peak load and failure energy. Moreover, failure mode effect on peak load and failure energy is not significant in nominal and large TRIP800 spot welds unlike the DP800 welds. As an example, it has been observed that large spot welds of TRIP800 failed in different failure modes had similar failure energy. Therefore, failure mode effect on mechanical performance of TRIP800 spot welds decreases with the increase of FZ size. According to the researchers, this difference is associated with the micro-hardness profile. Because two types of AHSS have different micro-hardness profiles and HAZ softening was only observed in DP800 spot welds. In addition, higher peak load and energy absorption capability were obtained typically with the increased FZ size. Hence, most important factor determining the weld quality was mentioned as FZ size in the study [24].

In 2022, DiGiovanni et al., investigated the liquid metal embrittlement (LME) severity in different types of galvanized AHSS sheets subjected to external loading to simulate the manufacturing conditions. LME is a known phenomenon observed in RSW of galvanized steels due to penetration of liquid Zinc to the solid boundaries of base metals. It results with loss of ductility particularly in electrode/sheet interface. It was mentioned the LME occurrence is sensitive to high temperature and stress. In the research, Galvanized, TRIP1100, TRIP690, DP980 specimens were externally loaded from the bottom sheets after the welding is completed since the scope of the research is to investigate the sensitivity of LME to loading. Experimental results showed the materials with highest inherent susceptibility to LME were more affected by external loading in terms of crack formation. The reasons for the LME susceptibility difference of the steels are grain structure characteristics and amount of Si content in their chemical composition. Sensitivity to LME was observed from least to greatest in DP980, TRIP690 and TRIP1100, respectively. Crack occurrence was initiated in TRIP1100 sheets with directly start of external loading. Crack severity in TRIP690 was increased with the load of %40 of yield strength of the material. However, for DP980, measurable crack index was achieved only above the load of %60 of yield strength. As a result, manufacturability of each material with different susceptibility to LME is different since the severe crack formation must be prevented [25].

Song et al., in 2022, searched the effects of expulsion and heat extraction on LME severity. Heat extraction and expulsion influence on LME was monitored with the change of electrode force. LME-sensitive galvanized 1.4 mm thick 3G-AHSS were used as base metal of the work. Spot welding of steel sheets was done at various heat input levels such as low, moderate and high heat input. Experimental method of the study was to change the electrode force along with the changing welding current, thus obtaining the same nugget diameter for each heat input level with the changing electrode force. Hence, electrode force influence on LME was monitored for each heat input level. Crack index which considers the frequency and length of the cracks together was used to rate the crack severity. Cracks from different regions of weld cross section such as electrode indent, weld shoulder and weld notch were classified as different crack types and the index of each crack type was monitored for each heat input level. It was observed that the total crack index, so that the LME crack severity, decreased with increasing electrode force at low heat input level. The reason for that is the increase in heat loss due to increased

contact area between the water-cooled electrodes and metal sheets as a result of electrode force increase. However, total crack index was not decreased with the increase of electrode force at moderate and high heat input levels. Because the LME severity was affected more by the expulsion and electrode collapse into the steel as the heat level increases. Ferro-static pressure of liquid metal in the nugget drops with the expulsion and results with sudden collapse of electrode into the metal. In the research, electrode sink into the sheets caused fast tensile deformation which was associated with severe crack formation. The other influence of expulsion on LME was associated with thermal stresses occurred in the weld shoulder as a result of rapid cooling caused by severe electrode indent increase. Since the electrode force increase resulted with severe electrode indentation at moderate and high heat input level, where the expulsion was observed, thermo-mechanical component of LME component was also triggered with the increased electrode force. Therefore, electrode force increase caused decreased LME crack severity in low heat input level because of increased heat extraction but also resulted with increased crack formation at moderate and high heat input levels where the heat extraction was not a dominant factor [8].

In 2018, innovative research covering expulsion analysis was presented by Mikno et al. The scope of the research was detection and elimination of expulsion with the aid of measuring and control system developed by the researchers. The measuring system, called LodWeld 4, was consist of sensors, a high-speed camera (10000 fps recording) and electronic module that synchronized process parameters such as welding current and voltage, electrode force and electrode travel. Process parameters recording and image recording were done simultaneously in spot welding process of 1 mm thick DP800 steel sheets. Invertor welding machine, with 10 kHz frequency, and controller using discrete differentiation algorithm were used to upgrade the resolution of the process so that expulsion could be eliminated with fast response. It was seen that most dynamic response was obtained from the electrode force waveform comparing the other process parameters. Therefore, welding time where the expulsion was occurred was read from the electrode force waveform, corresponding time to visible drop in electrode force, and it was seen that it matched with the expulsion time detected via image recording. In this way, response of the electrode force signal to the expulsion was tested. The necessity of using control system was explained with insufficient expulsion free nugget diameters (<5 mm using 7.5 kA) obtained via conventional waveform. Hence, control system was

implemented to the study in two stages. First, the current flow was stopped when expulsion initiation was detected with the discrete differential control algorithm and expulsion free welds were obtained. Because of the break in heat input, nugget diameters were insufficient at the end of the first stage. Then, after a break time, second pulse was applied with predetermined process parameters through multiple tests. It was seen that narrow nuggets, in which expulsion initiation was detected, can be enlarged in this method without observing any expulsion. Therefore, larger expulsion free nuggets (>5 mm) can be obtained compared to the conventional method. This control method provides insights to improve the weld quality thanks to expulsion elimination. It should be noted, further quality analysis such as microstructure and microhardness analysis on the spot welds using two pulse form was not provided by the researchers in this paper [26].

3. EXPERIMENTAL PROCEDURE

3.1 Sample Properties

In the experimental study of thesis, two steel sheets of same material were used for each spot welding. Base metal of RSW was 1 mm thick electrogalvanized DP steel DP800. Chemical composition of DP800 steel is given in Table 3.1.1.

Table 3.1.1 DP800 Chemical Composition (wt %)

C	Mn	Si	Cr	Ni	Al	Cu	P	S	Fe
0.145	2.13	0.184	0.259	0.045	0.028	0.028	<0.01	<0.01	Bal.

DP800 DP steel microstructure mainly consists of ferrite and martensite phases. Thanks to ferrite component, DP800 steel provides good formability. Besides of being formable, DP steels are also high strength steels because of their martensite structure and C, Mn, Cr rich composition. Offering high strength and formability features together is the reason of favorable usage of DP800. Mechanical properties of DP800 are listed below in Table 3.1.2. Mechanical properties of DP800 are given as the average of five tensile measurements.

Table 3.1.2 Mechanical Properties of DP800

Material	Yield Strength [MPa]	Tensile Strength [MPa]	Elongation [%]
DP800	718.40	922.33	16.63

3.2 Resistance Spot Welding Process

RSW sample was the DP800 steel sheet pair as aforementioned. Sample geometry can be seen in the Figure 3.2.1. Steel sheets with dimensions of 30.0x105.0x1 mm^3 were used in experimental studies.

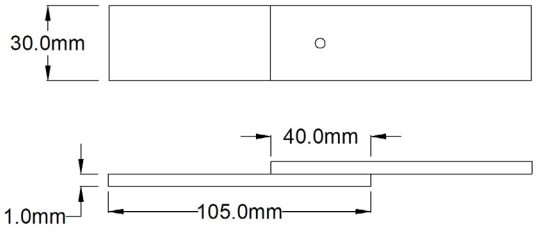

Figure 3.2.1 Top and side views of the RSW specimen

In order to prepare the steel sheets for spot welding, sheets were cleaned with acetone and then placed on a spot welding fixture. Steel sheets were overlapped of ~40 mm around the center of the fixture in the longitudinal direction, normal to the electrodes. All welding joints are generated using a computer numeric controlled pedestal type AC machine with a capacity of 70 kVA. Copper-based electrodes with dome-radius geometry and 6 mm face diameter were used in accordance with ISO 5821 standard in order to conduct the welding current through DP800 steel sheets. Both electrodes were actively cooled with a minimum flow of 12 liter/min.

Weld parameters are selected in accordance to American Welding Society (AWS) standards [27]. Electrode force is kept constant at 3.1 kN in all trials. Moreover, a welding time of 14 cycles have been selected. Approach time and hold time are selected as 50 cycles and 20 cycles, respectively. Welding current was varied between 6.5 kA to 12 kA with a step size of 0.5 kA. For each variation, 8 different welding samples are generated.

3.3 Resistance Spot Welding Sample Tests

Geometry, microstructure, and hardness is investigated in the cross section of the joints generated using varying current values. Samples are cut using abrasive disks in the middle section of the joint in transverse direction and cold mounted. All samples are first ground with sand papers in between P400 and P2500 grits. Afterwards, surface has been polished using 6μm and 1μm diamond suspension. Samples are etched with 4% Nital solution for 12 seconds. Geometry of the nugget is measured optically on the cross-section using Optika SLX-3 stereomicroscope. Furthermore, microstructure of different spots of the joint is investigated using Hitachi SU5000 scanning electron microscope (SEM). Microhardness of the welds have been measured according to ISO 6507 standard with a

load of 0.5 kgf and 15 seconds dwell time along a section above 0.2 mm of the faying surface of the joint. The distance between each measurement is selected as 0.20 mm.

Afterwards, mechanical properties of the welded joints are determined using tensile shear tests according to the ISO 14273 standard using UTEST servo-mechanical universal tensile test machine. Seven specimens have been tested for each welding current to be able to generate statistically meaningful results. Tensile shear strength and failure energy, which are measures of load bearing capacity and energy absorption capability, were analyzed by using tensile data to determine the mechanical properties of spot weld joints. Failure energy which corresponds to the stored energy in the joint up to the tensile-shear strength point is determined using a developed macro which is calculating the area covered by the load-displacement curve. Finally, fractured joints in tensile loading are visually controlled to investigate expulsion trace and failure mode which are the other characteristics determining the weld quality. Failure mode in the joints is investigated using Canon EOS 550D digital camera and Nikon Eclipse LV150 optical microscope.

4. RESULTS AND DISCUSSION

Results of the experimental studies have been discussed in this chapter. The chapter basically consist of microhardness and microstructure analysis, investigation of geometrical attributes of RSW joints, tensile-shear test results and failure mode analysis.

4.1 Microhardness and Microstructure Analysis

Excessive heating and rapid cooling operations are the part of RSW process. Therefore, multiple zones with different features are seen in the microstructure of a spot welded sample. In the thesis study, microhardness of a typical DP800 RSW sample was measured and microhardness distribution is given in the Figure 4.1.1. Furthermore, microstructure of the RSW sample was imaged from different zones using SEM. Micrographs of the sample are given in the Figure 4.1.2. Figure 4.1.2 illustrates the microstructure of the spot weld in four regions such as BM **(b)**, transition region from ICHAZ (inter-critical heat affected zone) to UCHAZ (upper-critical heat affected zone) **(c)**, UCHAZ **(d)** and finally the FZ **(e)**.

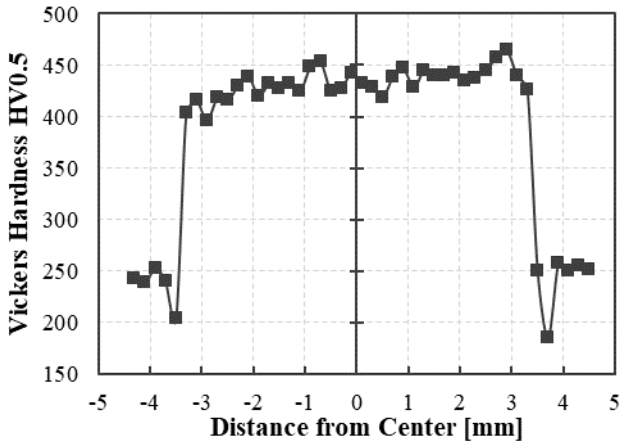

Figure 4.1.1 Microhardness profile of spot welded DP800 specimen

Figure 4.1.1 shows the microhardness distribution across the spot weld. As approached from outermost part towards the center in Figure 4.1.1, microhardness values of the BM, HAZ and FZ can be seen respectively. Microstructure of the DP800 steel BM consist of ferritic matrix with embedded martensite islands and has a microhardness around 250 HV. Since it is the section outside of the zone affected by the heat which is visible in the

Figure 4.1.2(a) with a yellow boundary, there is no phase transformation observed in this zone. Therefore, BM structure simply refers to original structure of the workpiece. The microhardness distribution of DP800 BM is in line with the literature since the DP600 and higher grade DP steels generally have microhardness values above 200 HV in their BM [1, 24].

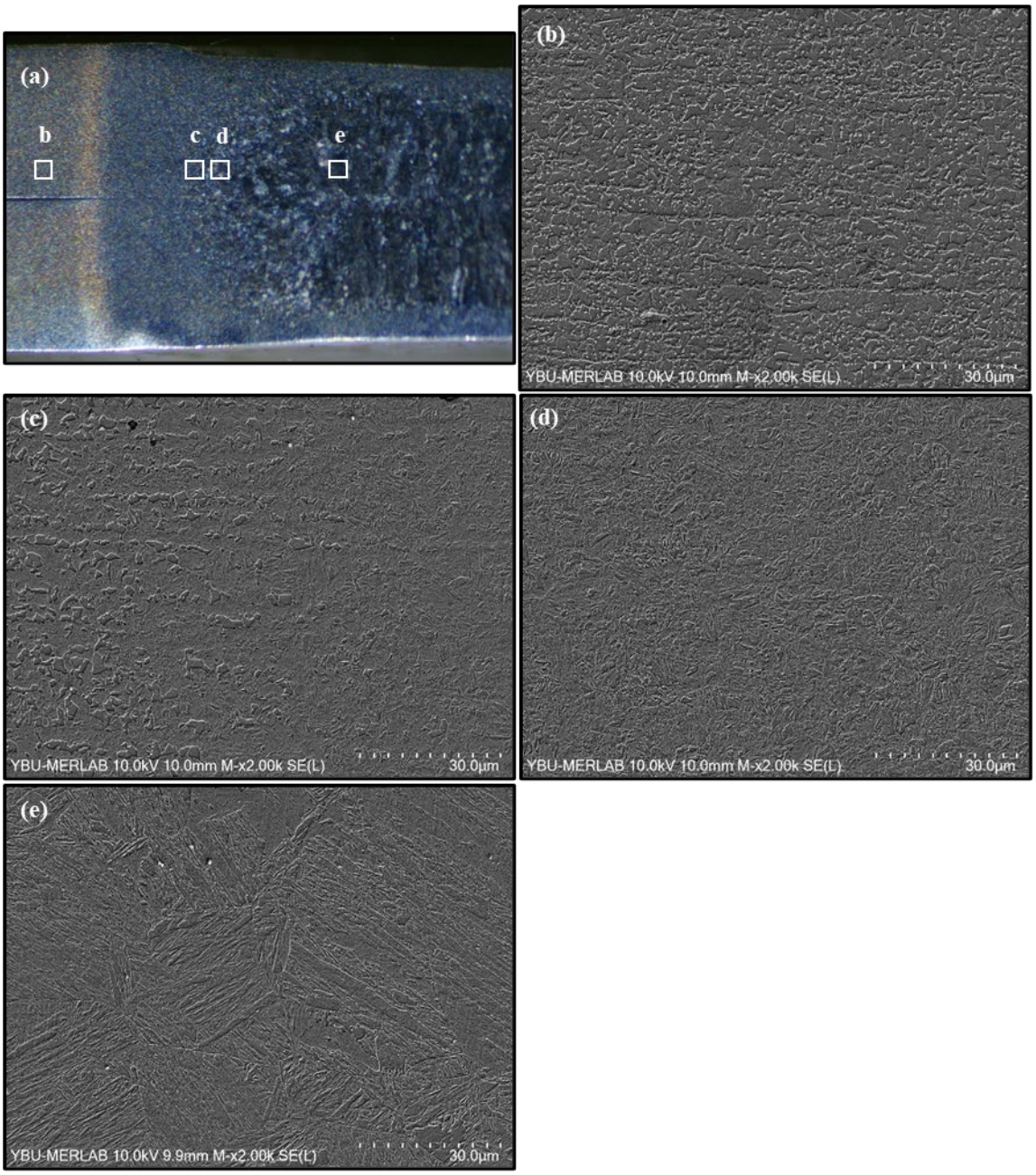

Figure 4.1.2 Micrographs of DP800 a) spot weld cross section b) base metal c) transition boundary of HAZ d) UCHAZ and e) FZ

Next to the BM, there is HAZ simply consists of two regions which are ICHAZ and UCHAZ. It is demonstrated in the Figure 4.1.1 the hardness values in ICHAZ, adjacent to the BM, are lower than the 250 HV. Thus, there is a softening in hardness profile when passing through this zone. The reason for the HAZ softening is tempering of the pre-existing martensite in the DP800 microstructure. In ICHAZ, peak temperature is between the lower critical temperature and upper critical temperature. In addition, volume fraction of pre-existing martensite is high in DP800. These are the reasons why the pre-existing martensite can be tempered. Microstructure of the ICHAZ of DP800 spot weld is mostly a multiphase structure. Various phases can be observed in the microstructure of the zone depending on the cooling rate which partially austenitized region is exposed.

In the hardness measurement of the study, hardness increase was observed when passing from the ICHAZ to UCHAZ due to increased martensite fraction in the microstructure. As seen in the Figure 4.1.1, microhardness of the HAZ was increased closer to the FZ. In UCHAZ, peak temperature is above the upper critical temperature. Therefore, structure of the BM transforms into austenite and then the austenite solidifies in a relatively high cooling rate. As a result, martensite fraction hence the hardness increases. In UCHAZ, grain growth occurs in varying amounts depending on duration of the heating above the upper-critical temperature. Thus, the region involves both of fine-grained and coarse-grained structures. Fine grained structure in UCHAZ of the DP800 spot weld specimen can be seen in the Figure 4.1.2(d) with growing grains closer to FZ.

In RSW, greatest peak temperatures and cooling rates can be seen in FZ. As a result of full austenization and rapid cooling, volume fraction of martensite increases significantly. Therefore, highest hardness values in the microhardness measurement were supplied by the FZ. As shown in the Fig 4.1.1, in the FZ of the sample, relatively uniform hardness profile was obtained and the hardness values are fluctuating around the 430 HV. In addition, martensite in the lath morphology was observed in the FZ of the sample due to quenching of fully austenitized structure. Columnar grain structure of martensite can be seen in the Figure 4.1.2(e).

4.2 Geometrical Attributes of Resistance Spot Welding Joints

Mechanical performance of spot welds is highly affected by the nugget geometry. Larger joints produced in same material are able to carry higher loads. Therefore, analysis of geometrical attributes of RSW joints is essential for weld quality investigation. The most

common geometrical features examined in a spot weld cross section are nugget width and electrode indentation. Therefore, these attributes were measured and results are given in Figure 4.2.1 and Figure 4.2.2 for the nugget width and electrode indentation, respectively.

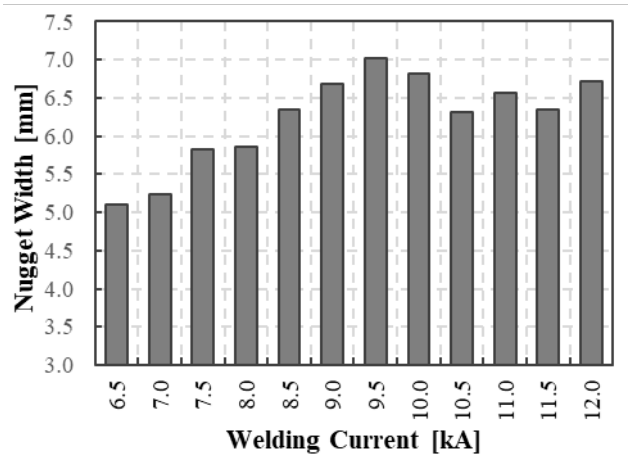

Figure 4.2.1 Nugget width by welding current

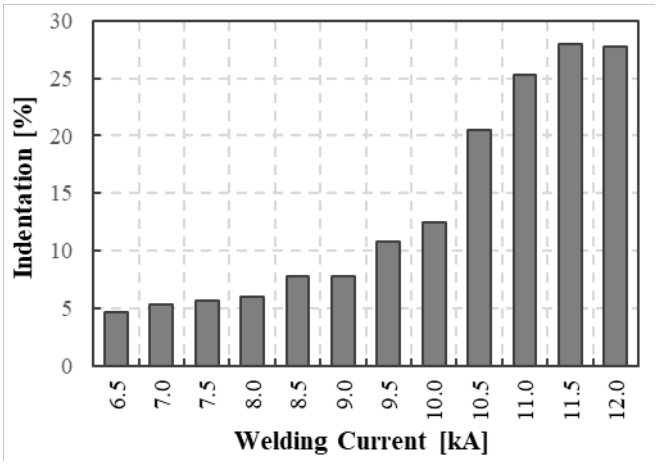

Figure 4.2.2 Welding current influence on electrode indentation

It should be noted that the terms nugget width and nugget diameter are interchangeable in the RSW. According to the standard [27], all of the RSW trials resulted in a satisfactory nugget formation, as all the samples have a nugget greater than 4.3 mm in diameter. It is seen in the Figure 4.2.1, the nugget width was increased, up to 7 mm, as the welding current increased from 6.5 kA through 9.5 kA. The reason for that is the higher heat input allowing larger nugget formation. However, despite the increased heat input, the nugget width was decreased due to severe expulsion and fluctuated around 6.5 mm when using welding current above 9.5 kA.

In the microscopy, expulsion was observed in the use of welding current above 9.0 kA. Moreover, the nugget diameter increase cannot be prevented by the expulsion when the

welding current increased from 9.0 kA to 9.5 kA. However, the expulsion is an undesired phenomenon in RSW and the nugget diameter obtained by using 9.0 kA is still quite satisfactory (6.7 mm). Microscope image of an expulsion example is given in the appendix 1.

In Figure 4.2.2, electrode indentation values are given as the percentage of the total sheet thickness. It is seen, the electrode indentation increased as the welding current increased. The reason for the gradual increase in the indentation up to welding current use of 9.0 kA is increase in heat input as a result of increase in welding current. Since the plastic deformation in the electrode-sheet surface is affected by the temperature of the surface, higher welding current usage results in deeper electrode sink.

In the use of welding current beyond 9.0 kA, there is an additional factor, other than the increasing heat input, invoked the rapid electrode sink which is the expulsion. Since the expulsion disrupts the mechanical equilibrium between the electrodes and molten metal, electrodes can easily indent to the metal sheets in case of expulsion. Therefore, a rapid increase in indentation (from %7.75 to %10.75 of total sheet thickness) was observed when the welding current was increased from 9.0 kA to 9.5 kA. Afterwards, the indentation increased rapidly (from %12.50 to %20.50 of total sheet thickness) when the welding current was increased from 10.0 kA to 10.5 kA due to increase in expulsion severity.

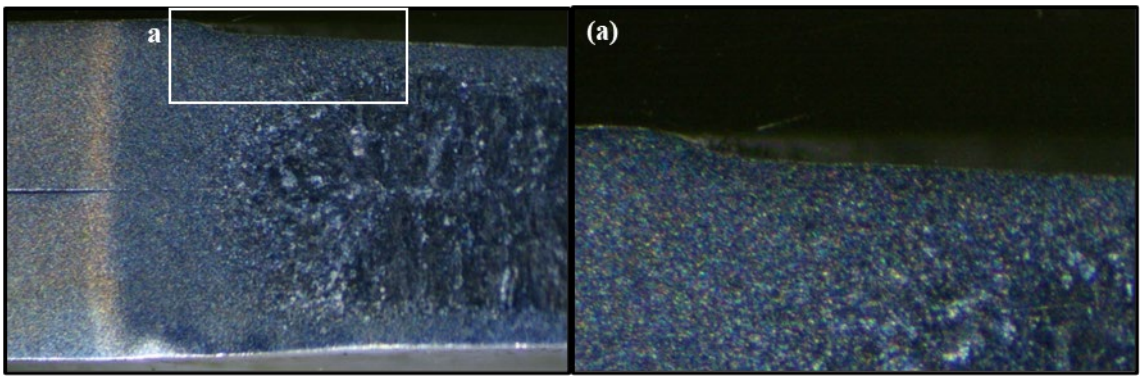

Figure 4.2.3 Microscope image of a weld sample a) electrode-sheet interface with no LME crack

In addition, LME crack occurrence in the samples was also investigated in the microscopy for each welding current level and no traces of LME crack were found. Figure 4.2.3 shows the microscope image of a weld joint and a closer look to electrode-sheet interface. As seen in the Figure 4.2.3(a), there is no LME crack on the spot weld sample electrode-

sheet interface. In addition, no crack formation is observed on the remaining contact surfaces of the sample. Furthermore, the LME crack status is the same for all of the RSW samples.

In brief, larger nugget width and lower electrode indentation are both associated with better weld quality since better mechanical properties can be achieved with the larger bond area in the FZ. Hence, optimal geometrical attributes on nugget cross section were met by using 9.0 kA.

4.3 Tensile Shear Test

The scope of the tensile shear test is to monitor the change of mechanical properties of RSW joints such as tensile shear strength and failure energy by current level. Figure 4.3.1 shows the average tensile shear strength and failure energy values, with embedded bars showing the deviation between maximum and minimum values, achieved using different welding currents for constant electrode force (3.1 kN) and weld time (14 cycle).

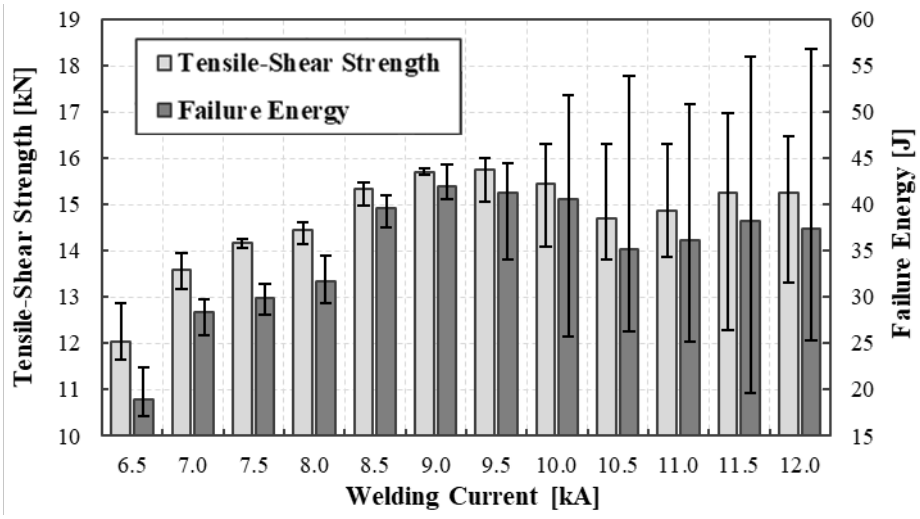

Figure 4.3.1 Mechanical properties of the spot welds by welding current

As seen in Figure 4.3.1, tensile-shear strength and failure energy of the spot welds increased with the increase of welding current from 6.5 kA through 9.0 kA. Further increase in welding current above 9.0 kA, resulted in a decrease of average values of mechanical properties. Moreover, high deviation between the maximum and minimum values of two mechanical properties was observed when the welding current exceeded 9.0 kA. Although, the maximum tensile-shear strength and failure energy values were

increased as the welding current increased, the average values in mechanical properties were decreased in the use of welding current above 9.0 kA because of the deviation. In brief, inconsistency has emerged in the mechanical properties of the joints generated using welding current above 9.0 kA.

The reason for the inconsistent mechanical properties within each welding current level above 9.0 kA and the high deviation is the expulsion triggered by excessive heat input. Since material escape from FZ results with inconsistent nugget formation, high deviation in mechanical properties of spot welds is inescapable in expulsion occurrence. Since the expulsion is still visible on fractured samples thanks to burning marks, samples were visually controlled after the tensile shear test in order to investigate the occurrence of expulsion. Expulsion was observed in half of the RSW samples generated using 9.5 kA welding current and all of the samples generated using welding current greater than 9.5 kA. Moreover, expulsion severity was also increased dramatically as the welding current further increased up to 12.0 kA. The number of samples exhibiting expulsion was insignificant when a welding current below 9.5 kA was used.

It was observed the failure energy is highly responsive to tensile-shear strength. Basically, larger changes occurred in the failure energy values in response to changes in tensile-shear strength since the failure energy is found by calculating the covered area by load-displacement curve up to tensile-shear strength point. Small increments in tensile-shear strength resulted in high improvement in energy absorption capability in the non-expulsion region, ≤ 9.0 kA. For instance, failure energy was increased 24% (from 31.7 J to 39.6 J) for only 6% (from 14.5 kN to 15.3 kN) tensile-shear strength improvement when the welding current was increased from 8.0 kA to 8.5 kA. Moreover, the deviations in tensile shear strength triggered the larger deviations in failure energy in the use of welding currents at which the expulsion experienced.

4.4 Failure Mode Analysis

Failure mode has significant influence on mechanical performance of spot welds and provides strong insights about the weld quality. RSW joints may fracture in various modes such as interfacial, partial interfacial and pullout failure modes when subjected to tensile loading. Generally, the interfacial failure mode indicates the insufficient nugget size and low energy-absorption capability while the pullout failure mode is associated with the high plastic deformation and high load carrying capacity. Since, the withdrawal

of the nugget from the base metal is a must in pullout failure mode, high plastic deformation is needed to fracture in this mode. However, the interfacial failure is the failure mode in which the failure is observed by rapid crack growth in the nugget through the longitudinal direction.

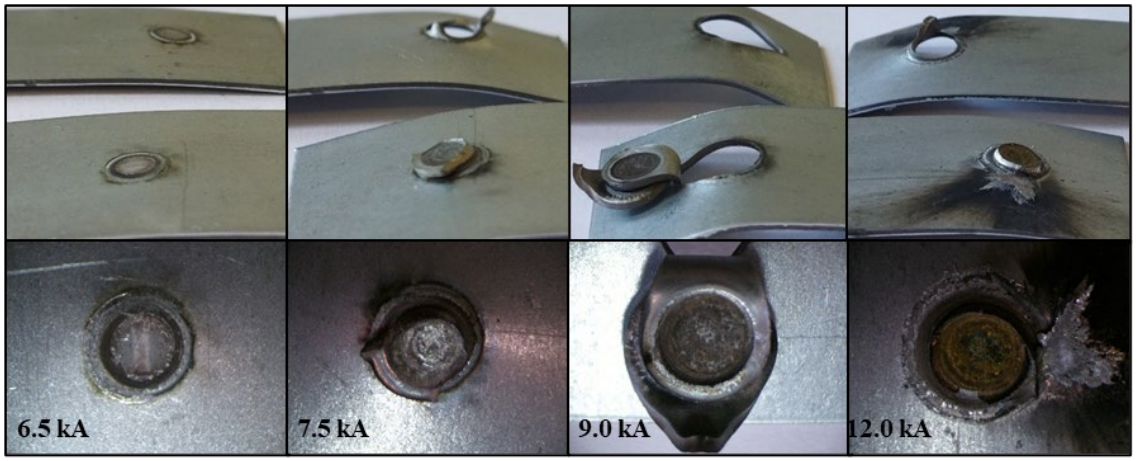

Figure 4.4.1 Failure modes of the RSW samples

All the three mentioned failure modes were observed in the experimental study. Figure 4.4.1 shows the failure modes of the samples subjected to tensile-shear test. From left to right, interfacial failure, partial interfacial failure, double-sided pullout failure and single-sided pullout failure were occurred in the samples respectively. Welding currents applied to weld the sheets are mentioned at the bottom left of the microscope images for each type of failure. As seen in the Figure 4.4.1, tendency of the samples to pullout mode increases as the welding current and therefore the nugget size increases.

Spot weld sample using 6.5 kA current failed in the interfacial mode while the partial interfacial failure was observed in the joint using 7.5 kA current. In the interfacial failure mode, crack propagates completely along the longitudinal direction of the FZ while in the partial interfacial failure mode, the crack propagation starts in the longitudinal direction but then propagation course changes through the transverse direction. This is why partially pulled nugget is seen in this mode.

Joints obtained using 9.0 kA and 12.0 kA welding currents fractured in double-sided pullout and single-sided pullout failure modes, respectively. The reason for the transition from the double-sided failure to single-sided failure is decreased nugget size caused by the expulsion. As seen in the Figure 4.4.1, there is a severe expulsion at the RSW sample at which 12.0 kA welding current is applied.

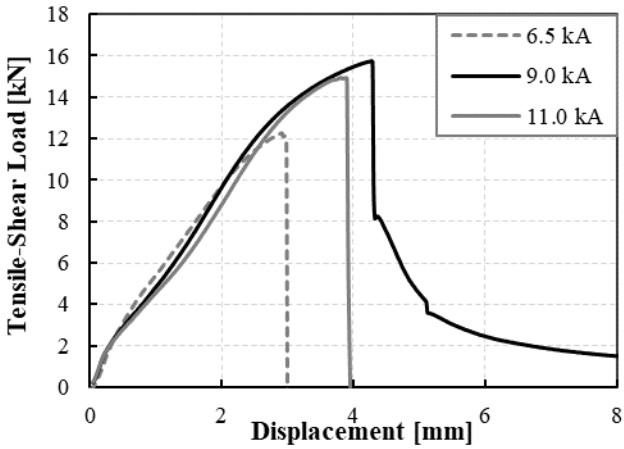

Figure 4.4.2 Load-displacement curves of RSW samples obtained with different welding currents

Figure 4.4.2 shows load-displacement curves of several joints, related to different failure modes, subjected to tensile loading. Tensile data given in the Figure 4.4.2 belong to different samples than the samples imaged in the Figure 4.4.1. Samples exhibiting characteristic tensile data were chosen in order to explain the issue better. As seen in the Figure 4.4.2, mechanical properties of the spot welds are affected by the welding current. As a result of increase in welding current, course of the load-displacement curves was changed. However, maximum peak load and failure energy values could not be reached by using highest welding current, 11.0 kA.

Interfacial failure occurred in the sample using 6.5 kA welding current and transition of the failure mode to double-sided pullout failure mode was observed when the welding current increased to 9.0 kA. Therefore, the peak load of the spot weld increased from 12.3 kN to 15.7 kN. In double-sided pullout failure mode, the reason for achieving the highest peak load is the larger nugget size. Afterwards, when welding current further increased to 11.0 kA, failure mode was changed to single-sided pullout failure. Due to severe expulsion and hence reduction in nugget size, peak load value decreased slightly, to 15 kN, in comparison to the double-sided failure.

In addition, failure energy in the joints was increased as the nugget size and therefore the peak load was increased. Greatest failure energy was obtained in the joint failed in double-sided pullout failure mode. Failure energy values of the samples welded using 6.5 kA, 9.0 kA, 11.0 kA are 20.72 J, 40.61 J and 32.13 J, respectively. In brief, double-sided pullout failure is the expected failure mode to achieve improved mechanical properties in the joints.

5. SUMMARY AND OUTLOOK

In the thesis study, electrogalvanized DP800 steel sheets with dimensions of 30.0x105.0x1 mm^3 were successfully welded by using RSW method. RSW method was carried out by applying varying welding parameters between 6.5 kA and 12.0 kA, with a step size of 0.5 kA, while the electrode force (3.1 kN) and weld time (14 cycle) kept constant. Afterwards, geometrical and mechanical attributes of weld joints were investigated in order to analyze the effect of changing welding current on weld quality. The conclusions from the research are as follows:

1. Microhardness of the DP800 joints is enhanced in the FZ, hardness is around 430 HV, thanks to martensitic structure achieved by austenitic transformation and subsequent rapid cooling. Besides, HAZ softening was observed in the ICHAZ of the joint microstructure due to tempering of pre-existing martensite.

2. Microscopic investigation indicates that satisfactory nugget width (>4.3 mm) was obtained according to the AWS standard [27] at all levels of welding current use, from 6.5 kA to 12.0 kA. Moreover, optimum geometrical attributes in the joints such as larger nugget width and lower electrode indentation were both achieved by applying 9.0 kA welding current. Further increase in welding current triggered the severe expulsion and therefore the nugget geometry was disrupted.

3. In microscopy, no traces of LME crack occurrence were found in the samples.

4. Tensile-shear strength as well as the failure energy of the DP800 joints were improved by increasing welding current up to expulsion limit, 9.0 kA. In the use of welding current above 9.0 kA, large deviation was observed in the mechanical properties of the joints due to expulsion. Expulsion occurred in half of the joints generated by applying 9.5 kA welding current and in all of the joints in which larger welding current was used.

5. Since the tendency to pullout failure mode increases as the nugget size increases, better mechanical performance in weld joints was achieved with the pullout failure mode compared to the interfacial failure mode. Greatest mechanical properties were

obtained in double-sided pullout failure mode by using 9.0 kA welding current. In addition, failure mode transition from double-sided pullout failure mode to single-sided pullout failure mode was observed, due to expulsion, when the welding current further increased. As a result of the transition to the single-sided pullout failure mode, mechanical properties of the joints were weakened.

6. As a conclusion, welding current has a significant influence on mechanical properties of the joints and weld quality, as it has a great impact on heat generation mechanism in the RSW joints and hence the nugget formation. In addition, optimum geometrical attributes and mechanical properties in the joints were obtained by applying 9.0 kA welding current in the RSW of 1 mm thick electrogalvanized DP800 sheets.

It is an effective procedure to select the welding current as the varying welding parameter since many outcomes could be achieved by only monitoring the effect of welding current on nugget formation and weld quality. As a further study, it would be recommended to increase the complexity of welding parameters with an additional weld time scale to observe if the weldability of DP800 joints is improved. Furthermore, different types of electrode geometries can be used with the optimum combination of welding current and weld time in order to observe if the weld quality of DP800 joints is improved further.

6. REFERENCES

[1] Jaber, H. L., Pouranvari, M., Salim, R. K., Hashim, F. A., & Marashi, S. P. H. (2017). Peak load and energy absorption of DP600 advanced steel resistance spot welds. Ironmaking and Steelmaking, 44(9), 699–706. https://doi.org/10.1080/03019233.2016.1229880

[2] Intranmx. (2021, Feb 19). Spot welding pros and cons. Intran - the Right Level. https://www.intran.mx/spot-welding-pros-and-cons/ (Date of Access: 2024, Feb 27)

[3] Chabok, A., Cao, H., van der Aa, E., & Pei, Y. (2022). New insights into the fracture behavior of advanced high strength steel resistance spot welds. Journal of Materials Processing Technology, 301. https://doi.org/10.1016/j.jmatprotec.2021.117433

[4] Shi, S. |. W. S. (2003). Resistance spot welding of high strength steels. https://www.twi-global.com/technical-knowledge/published-papers/resistance-spot-welding-of-high-strength-steels-may-2003 (Date of Access: 2024, Feb 27)

[5] Zhang, H., & Senkara, J. (2005). Resistance Welding. CRC Press.

[6] Chertov, A. M., & Maev, R. G. (2005). A one-dimensional numerical model of acoustic wave propagation in a multilayered structure of a resistance spot weld. IEEE Transactions on Ultrasonics Ferroelectrics and Frequency Control, 52(10), 1783–1790. https://doi.org/10.1109/tuffc.2005.1561632

[7] Kimchi, M., & Phillips, D. H. (2023). Resistance Spot Welding. Springer International Publishing.

[8] Song, S., Shojaee, M., Midawi, A. R. H., Sherepenko, O., Ghassemi-Armaki, H., & Biro, E. (2023). Influence of expulsion and heat extraction resulting from changes to electrode force on liquid metal embrittlement during resistance spot welding. Journal of Materials Research and Technology, 23, 1458–1470. https://doi.org/10.1016/j.jmrt.2023.01.093

[9] O'Brien, A., & Guzman, C. (2007). Welding handbook. Volume 3, Welding processes. Part 2.

[10] Colombo, T., dos Santos, G., Teruel, P., Otubo, J., & Faria, A. (2018). Microstructure evolution and failure modes of a resistance spot welded TWIP steel. Soldagem e Inspecao, 23(4), 460–473. https://doi.org/10.1590/0104-9224/SI2304.02

[11] Zhang, H., & Senkara, J. (2011). Resistance Welding: Fundamentals and Applications, second edition. CRC Press.

[12] ASM International Handbook Committee. (2011). ASM Handbook: Welding Fundamentals and Processes, Volume 6A. ASM International.

[13] Resistance Spot Welding Applications | It's not just for automobiles. (n.d.). Joining Technologies. https://joiningtech.com/resistance-spot-welding-applications-its-not-just-for-automobiles/ (Date of Access 2024, Mar 11)

[14] Resistance Spot welding Archives. (n.d.). AMADA WELD TECH. https://amadaweldtech.com/applications/methods/spot-welding/ (Date of Access 2024, Mar 11)

[15] WELDING SERVICES. (n.d.). ABC Sheet Metal. https://www.abcsheetmetal.com/welding-services/ (Date of Access 2024, Mar 11)

[16] World Auto Steel. (n.d.). Advanced High-Strength Steel (AHSS) Definitions https://www.worldautosteel.org/steel-basics/automotive-advanced-high-strength-steel-ahss-definitions/ (Date of Access 2024, Mar 13)

[17] World Auto Steel. (n.d.). RSW of Advanced High-Strength Steels. https://ahssinsights.org/joining/resistance-welding-processes/resistance-spot-welding/rsw-of-advanced-high-strength-steels/ (Date of Access 2024, Mar 14)

[18] Sivaraj, P., Seeman, M., Kanagarajan, D., & Seetharaman, R. (2020). Influence of welding parameter on mechanical properties and microstructural features of resistance spot welded dual phase steel sheets joint. Materials Today: Proceedings, 22, 558–562. https://doi.org/10.1016/j.matpr.2019.08.201

[19] Shen, J., Zhang, Y. S., & Lai, X. M. (2011). Effect of electrode force on expulsion in resistance spot welding with initial gap. Materials Science Forum, 675 677, 795–798. https://doi.org/10.4028/www.scientific.net/MSF.675-677.795

[20] Hwang, I. S., Kang, M. J., & Kim, D. C. (2011). Expulsion reduction in resistance spot welding by controlling of welding current waveform. Procedia Engineering, 10, 2775–2781. https://doi.org/10.1016/j.proeng.2011.04.461

[21] Chen, T., Ling, Z., Wang, M., & Kong, L. (2020). Effect of a slightly concave electrode on resistance spot welding of Q&P1180 steel. Journal of Materials Processing Technology, 285, 116797. https://doi.org/10.1016/j.jmatprotec.2020.116797

[22] Pouranvari, M., & Marashi, S. P. H. (2011). Failure mode transition in AHSS resistance spot welds. Part I. Controlling factors. Materials Science and Engineering: A, 528(29–30), 8337–8343. https://doi.org/10.1016/j.msea.2011.08.017

[23] Liang, J., Zhang, H., Qiu, X., & Shi, Y. (2015). Characteristics of the resistance spot welding joints in dissimilar thickness dual-phase steels. ISIJ International, 55(9), 2002–2007. https://doi.org/10.2355/isijinternational.isijint-2015-151

[24] Sun, X., Stephens, E. v., & Khaleel, M. A. (2008). Effects of fusion zone size and failure mode on peak load and energy absorption of advanced high strength steel spot welds under lap shear loading conditions. Engineering Failure Analysis, 15(4), 356–367. https://doi.org/10.1016/j.engfailanal.2007.01.018

[25] DiGiovanni, C. W., Shojaee, M., Biro, E., & Zhou, N. Y. (2022). Effect of external loading on liquid metal embrittlement severity during resistance spot welding. Manufacturing Letters, 33, 11–14. https://doi.org/10.1016/j.mfglet.2022.06.003

[26] Mikno, Z., Pilarczyk, A., Korzeniowski, M., Kustroń, P., & Ambroziak, A. (2018). Analysis of resistance welding processes and expulsion of liquid metal from the weld nugget. Archives of Civil and Mechanical Engineering, 18(2), 522–531. https://doi.org/10.1016/j.acme.2017.08.003

[27] American Welding Society (AWS) C1 Committee on Resistance Welding. (2019). Recommended Practices for Resistance Welding (AWS C1.1M/C1.1:2019). https://pubs.aws.org/

APPENDIX

APPENDIX 1 – Microscope Image of a Spot Weld Cross Section

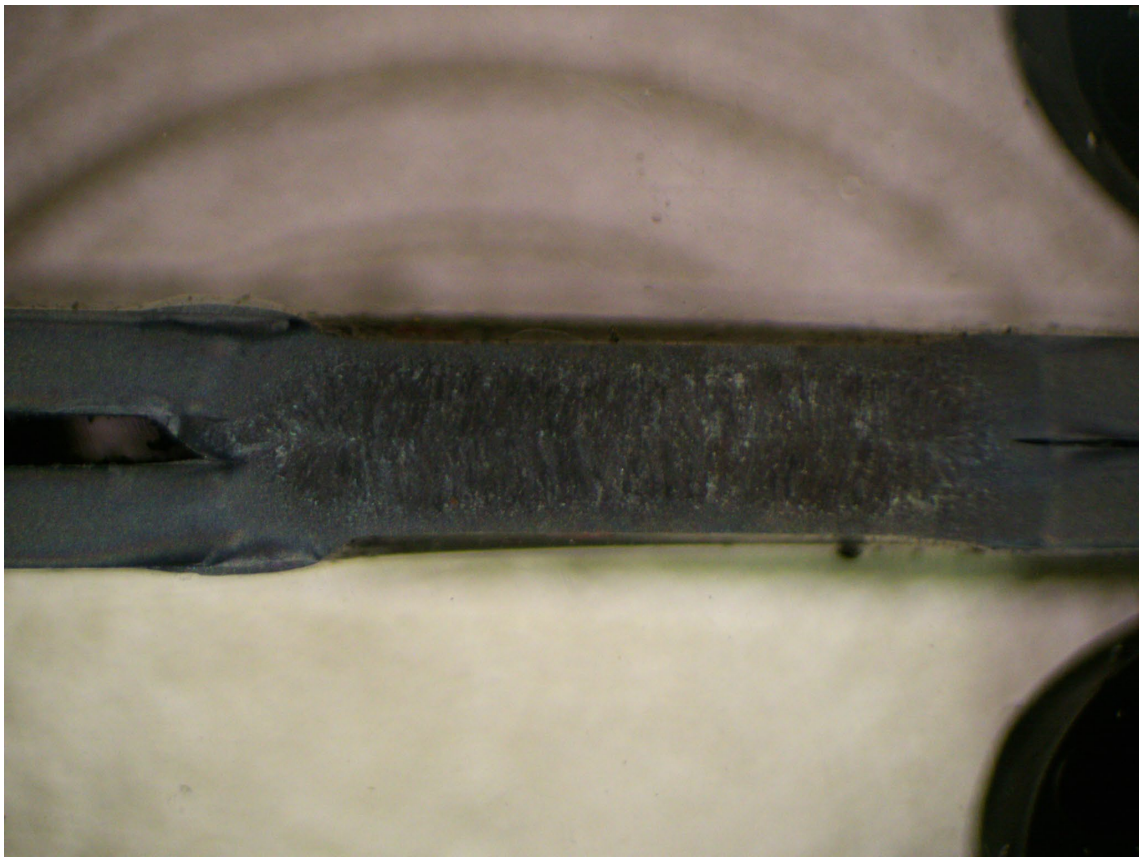

Figure A.1 Expulsion in a spot weld sample generated using 9.5 kA welding current

APPENDIX 2 – Resistance Spot Welding Data Sheet

EQUIPMENT PROPERTIES	
Type	Pedestal Type AC Spot Welding Machine
Control	Computer Numeric Control
MATERIAL PROPERTIES	
Type	Electrogalvanized DP Steel
Grade	DP800
Thickness [mm]	1.00
Surface Condition	Solvent applied
Yield Strength [Mpa]	718.40
Tensile Strength [Mpa]	922.23
Elongation at Fracture [%]	16.63
ELECTRODE	
Geometry	Dome-radius
Face Diameter [mm]	6
WELDING PARAMETERS	
Current Range [kA]	6.5 to 12
Approach Time [cyc]	50
Weld Time [cyc]	14
Hold Time [cyc]	20
Pulse Count	1
Electrode Force [kN]	3.1
Overlap [mm]	40
WELD	
Nugget Width [mm]	>5
Indentation [% of total sheet thickness]	>5
Expulsion Occurence [Y/N]	Y- Current use above 9.0 kA

Table A.1 Resistance spot welding data sheet